

First Excited State Properties and Static Hyperpolarizability of Ruthenium(II) Ammine Complexes

Talgat M. Inerbaev,* Rodion V. Belosludov, Hiroshi Mizuseki, Masae Takahashi, and Yoshiyuki Kawazoe

Institute for Materials Research, Tohoku University, 2-1-1 Katahira, Aoba-ku, 980-8577 Sendai, Japan

Received August 4, 2005

Abstract: First principles calculations were used to study the electronic excitation energies (E), transition dipole moments (μ), and difference of dipole moments between ground and excited states ($\Delta\mu$) for low-lying singlets of the series of ruthenium(II) ammine complexes. Both cases of the gas phase and the acetonitrile solution were investigated in order to explain the discrepancy between the recent experimental and theoretical results and to develop the optimal way of estimation for the first static hyperpolarizability in the framework of a two-state model introduced by Oudar and Chemla. The present calculations reveal that the effect of solvent on the electronic properties of investigated compounds is not only the change of the excitation energy but also the increasing of ground-state molecular polarization and intensification of metal-to-ligand intramolecular charge transfer for electronic excitations. These effects lead to increasing of the values of $\Delta\mu$ and ground-state dipole moment μ_g in solution as compared with the gas-phase ones. The proposed theoretical approach gives good agreement with experiment and allows one to apply it for designing a new perspective nonlinear optical active organometallics.

Introduction

The design of new molecular materials with large second-order nonlinear optical properties (NLO) is currently the subject of extensive investigations by theoretical and experimental methods, since they are expected to be used as frequency doubler, electro-optic modulator, and photorefractive media.^{1–3} Within this field, an increasing amount of attention has recently been paid to organotransition-metal complexes which offer possibilities for combination of NLO effects with many superior characteristics, such as ultrafast response times, lower dielectric constants, better processability as thin-film devices, and enhanced nonresonant NLO responses.³ Besides organic molecules, organometallic structures are intriguing candidates as second-order NLO chromophores since⁴ (1) they show very strong absorption bands (metal-to-ligand charge transfer and ligand-to-metal charge transfer) that are related to high transition dipole moments

and low transitions energies; (2) organometallic and coordination compounds are often strong oxidizing or redoxing agents, since the metal centers may be electron rich or poor depending on their oxidation state and ligand environment [Thus, the metal center may be an extremely strong donor or acceptor.]; and (3) metals can be used to fine-tune the electronic properties of organic fragments.

A lot of organometallic and coordination compounds with a variety of metals, ligands, and molecular configurations were designed and synthesized. Their structures and NLO properties of the second and third order were studied.^{5–8} Usually, chromophores possessing large molecular hyperpolarizability β contain donor (D) and acceptor (A) groups linked through a π -backbone. The NLO properties of such polarizable dipolar compounds are caused by intense, low-energy $D(\pi) \rightarrow A(\pi^*)$ intramolecular charge-transfer (ICT) transitions. In the case of unidirectional ICT transition the frequency-independent nonresonance first hyperpolarizability β_0 can be described by a simple two-state model (TSM) introduced by Oudar and Chemla⁹

* Corresponding author phone: +81-(0)22-215-2057; fax: +81-(0)22-215-2052; e-mail: talgat@imr.edu.

$$\beta_0 = \frac{3\Delta\mu(\mu)^2}{E^2} \quad (1)$$

where μ is the transition dipole moment between ground and excited states, $\Delta\mu$ is the dipole moment change, and E is the energy gap between ground and excited states.¹⁰

A number of ruthenium(II) NLO active complexes were studied in detail using hyper-Rayleigh scattering and Stark spectroscopy techniques.^{11–14} There were established that NLO properties of these compounds are caused by strong metal-to-ligand charge transfer (MLCT). Moreover, the strong solvatochromic effect was demonstrated and the validity of TSM was proved.¹⁵ In the present paper we will study ruthenium(II) ammine complexes **1–4** presented in Figure 1, to propose the reliable theoretical description of NLO properties of organometallic and coordination compounds.

Theoretical quantum investigations are very helpful to study NLO chromophores. For example, a semiempirical computational study of (4-Y-pyridine)Cr(CO)₅ and (4-Y-stilbazole)Cr(CO)₅ was carried out by Kanis et al.¹⁶ The computed molecular hyperpolarizabilities were in good agreement with the Electric-Field-Induced-Second-Harmonic-Generation-determined experimental values. For ruthenium complexes such semiempirical calculations demonstrated the poor quantitative agreement with experimental data, and the best accuracy for $\Delta\mu$ and μ calculations was achieved about 25%.¹¹ The most recent experimental and theoretical study of the effects of polyene chain extension on the NLO properties of ruthenium(II) pyridyl complexes was done.¹³ The study based on B3P86^{17,18} hybrid functional with the LanL2DZ basis set in the gas phase gave rise to only a qualitative description of experimentally observed trends. Moreover, these calculations predicted that the change in dipole moment caused by the low-energy MLCT decreases with the polyene bridge length growth that is opposite to the experimentally observed tendency. Molecular first hyperpolarizabilities could be calculated by the finite-field (FF) method that involves a double numerical differentiation of the dipole moment with respect to the applied electric field, but the FF approach does not provide a microscopic interpretation of the obtained results.

In the present study, we have examined a time-dependent (TD) B3P86 functional approach to investigate the excited-state properties E , $\Delta\mu$, and μ of ruthenium(II) ammine complexes **1–4** (see Figure 1). The solvent effect on these characteristics has also been studied in order to understand the properties of investigated organometallic chromophores in details. Dependences on the choice of both the structure optimization method and the wave function basis set for TD-B3P86 analysis were also studied.

Computation Details

All theoretical calculations were carried out by the Gaussian 03 program.¹⁹ The geometry optimization of investigated structures was performed in the gas phase using HF, B3P86, and MP2 methods with the LanL2DZ basis set and by HF and B3P86 levels using a larger basis set, including LanL2DZ for Ru atom and 6-311++g(d,p) for N, O, C, and H atoms.

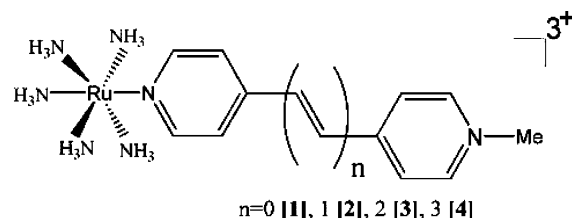


Figure 1. Chemical structures of cations investigated.

The solvent effect was estimated by performing calculations within the framework of the integral equation formalism polarized continuum model (PCM) developed by Tomasi.²⁰ Solute structure optimization was carried out by the HF/LanL2DZ approach. Electronic transitions were calculated by means of the TD-B3P86 method for all optimized structures using the same basis set that one used for optimization calculations. The HF/LanL2DZ gas-phase optimized structures were also analyzed by the TD-B3P86 theory using the 6-311++g(d,p)/LanL2DZ combined basis set. These data were compared with the data calculated for the HF/6-311++g(d,p)/LanL2DZ optimized structures in order to examine dependence of electronic excitation properties on the choice of the basis set for geometry optimization. To estimate the effect of the Ru(NH₃)₅-ligand distance variation on the electronic excitation properties, structure **2** was optimized in the gas phase employing the CEP-4G basis set on Ru and LanL2DZ on all other atoms. The choice of the B3P86 functional was based on the more accurate TD-B3P86 results provided by this functional when compared to the more widely used B3LYP functional.²¹ The differences of dipole moments between the ground and the n th excited states were estimated using the FF calculations (± 0.001 au) and the TD-B3P86 excitation energies,²² and the results were compared with data obtained by one particle RhoCI density. Experimental studies of investigated systems were carried out in acetonitrile (MeCN) at room temperature and butyronitrile (PrCN) at 77 K.^{11–14} Since at the present time modeling in the PrCN solution is unavailable in the Gaussian 03 program, we restrict ourselves to study systems in MeCN at zero temperature. Only electronic excitation properties were investigated, and for this reason the effect of zero-point energy correction was not estimated. Net atomic charges were calculated using the natural population analysis (NPA) included in the natural bond orbital algorithm proposed by Weinhold and co-workers.^{23–25} NPA analysis was carried out for the HF/LanL2DZ optimized structures by the B3P86/LanL2DZ method. NPA for excited states was performed using one particle RhoCI density. The default Gaussian 03 parameters were used in every case.

Results and Discussion

Geometry Optimization. Since up to the present there were not published crystallographic data of any salt containing the considered Ru(II) ammine complexes, we can perform only an indirect accuracy evaluation of the different methods of molecular geometry optimization by comparison of the theoretical estimation of electronic excitations with experimentally measured ones. It should be mentioned that the most important geometry parameter for push–pull chromophores

Table 1. BLA and Ru(NH₃)₅-Ligand Distances for Structures 1–4 Calculated by Different Theoretical Methods

compd	geometry parameter	6-311++g(d,p)/LanL2DZ		LanL2DZ			
		HF	B3P86	HF	HF/MeCN	B3P86	MP2
1	Ru(NH ₃) ₅ -ligand	2.296	2.109	2.278	2.219	2.083	2.161
2	BLA	0.152	0.114	0.141	0.145	0.105	0.115
	Ru(NH ₃) ₅ -ligand	2.275	2.105	2.258	2.316	2.083	2.152
3	BLA	0.137	0.095	0.127	0.129	0.089	0.096
	Ru(NH ₃) ₅ -ligand	2.256	2.107	2.245	2.248	2.088	2.147
4	BLA	0.131	0.083	0.120	0.113	0.078	0.089
	Ru(NH ₃) ₅ -ligand	2.246	2.107	2.237	2.375	2.091	2.144

responsible for their optical properties is the bond length alternation (BLA) defined as the average difference in the length between single and double bonds in the π -conjugated backbone.^{26–27} To study dependence on the geometry optimization method, compounds 1–4 were optimized in the gas phase at HF, B3P86, and MP2 levels using the LanL2DZ basis set. As it will be shown below, the TD-B3P86 calculations using the HF optimized molecular structures give the best agreement with experiment. For this reason and since the MP2 approach has a very high computation cost, the optimization using the 6-311++g(d,p)/LanL2DZ basis sets combination was carried out only by the HF and the B3P86 methods. The data of calculated BLA and Ru(NH₃)₅-ligand bond length values of compounds 1–4 are summarized in Table 1.

Most of the results presented in this study were performed using the structures optimized in the gas phase. Solution geometry optimization was carried out only by the HF/LanL2DZ approach, and in this case the optimization procedure with used parameters did not converge completely. The values of maximal and residual mean square displacements converged to values less than the corresponding default thresholds, but the same values of forces did not. All nonconverged forces are between Ru and surrounding it are nitrogen atoms and only partial optimization with converged values of displacement and significantly large values of ruthenium–nitrogen interatomic forces. Therefore, the solvent effect on the structural properties of investigated organometallics was not studied in detail such as for the gas-phase optimized geometries. The selected interatomic distances for structures 1 and 4 obtained for all considered cases are presented in Table 2. It can be pointed out that optimization in solution does not significantly affect the geometry of studied molecular complexes. Full geometry optimization of transition-metal complexes in solution using the PCM model needs additional contrivances, and this problem is beyond the boundaries of this study.

Electronic Excitations and NLO Properties. The values of E , μ , and $\Delta\mu$ for the first excited states were calculated by the TD-B3P86 method and compared with experiment.^{11–14} Selected calculation results are plotted in Figure 2. Data obtained for all molecular geometries considered in this study are presented in Table 3. To compare the theoretical and experimental results correctly it is necessary to denote that the MLCT bands of investigated chromophores undergo marked red-shifts with decreasing temperature.¹⁴ The measured changes in E on moving from 298 to 77 K are -0.15

and -0.23 eV for complexes 1 and 2 in the PrCN solution, correspondingly. At the same time, the values of oscillator strength that are directly related to the transition dipole moment μ show very little temperature dependence ($\leq 5\%$).¹¹

Calculations demonstrate that results are sensitive to the method of molecular structure optimization. Namely, for B3P86/LanL2DZ and MP2/LanL2DZ optimized structures the values of E and $\Delta\mu$ are in good agreement with data obtained by Stark spectroscopy (SS) measurements, and an error for values μ are found.^{12,13} Using the HF/LanL2DZ optimized structures, E and μ values were obtained in good agreement with the SS experiment, but $\Delta\mu$ values are overestimated. In both cases the values of μ and $\Delta\mu$ calculated for all structures demonstrate similar functional behavior. The value of E is a steadily decreasing function of n for B3P86/LanL2DZ and MP2/LanL2DZ optimized structures, while the experimental one is approximately constant for $n > 1$. From this point of view HF/LanL2DZ optimized structures give a better agreement with the experiment.

Calculations using the 6-311++g(d,p)/LanL2DZ combined basis set reveal the same qualitative results but with significant quantitative differences. In this case the values of E and $\Delta\mu$ are larger, and μ is smaller than the same values calculated using the LanL2DZ basis set. For the HF optimized structures the calculated E demonstrates perfect agreement with the room-temperature UV–visible absorption (VA) experiment except for the overestimated value for cation 1. At the same time for the B3P86 optimized structure 1 E is also overestimated, and for other compounds the calculated excitation energies are between SS and VA measured values. These results are not very sensitive to the variation of basis sets used for molecular structure optimization. Data obtained by 6-311++g(d,p)/LanL2DZ basis set TD-B3P86 analysis for HF/LanL2DZ and HF/6-311++g(d,p)/LanL2DZ optimized structures are qualitatively the same with some small quantitative difference. Employing larger basis set leads to an increasing of E and $\Delta\mu$ with a simultaneous decreasing of μ . We expect the same basis set dependence for structures optimized by the MP2 method that will not give a better agreement between experimental and theoretical results. Besides the reducing of the absorption energy there is also the effect of solvent on the electronic properties of investigated complexes. Gas-phase calculations predict that the change of dipole moment $\Delta\mu$ decreases with the polyene chain length growth. However, the study of these

Table 2. Selected Interatomic Distances (Å) for Structures **1(a)** and **4(b)** Calculated by Different Theoretical Methods^a

bond	B3P86/6-311++g(d,p)/ LanL2DZ	HF/6-311++g(d,p)/ LanL2DZ	B3P86/ LanL2DZ	MP2/ LanL2DZ	HF/ LanL2DZ	HF/ LanL2DZ/MeCN
------	---------------------------------	------------------------------	-------------------	-----------------	----------------	---------------------

C ₁ –N ₁	1.480	1.491	1.495	1.530	1.507	1.500
C ₂ –N ₁	1.347	1.334	1.362	1.383	1.348	1.350
C ₆ –N ₁	1.347	1.334	1.363	1.383	1.348	1.349
C ₂ –C ₃	1.379	1.374	1.391	1.415	1.383	1.384
C ₅ –C ₆	1.379	1.374	1.390	1.414	1.383	1.384
C ₃ –C ₄	1.399	1.391	1.412	1.431	1.401	1.406
C ₄ –C ₅	1.399	1.391	1.412	1.431	1.401	1.407
C ₄ –C ₇	1.480	1.496	1.484	1.505	1.494	1.517
C ₇ –C ₈	1.397	1.389	1.411	1.431	1.399	1.402
C ₇ –C ₁₁	1.397	1.389	1.411	1.431	1.399	1.400
C ₈ –C ₉	1.384	1.381	1.395	1.419	1.390	1.415
C ₁₀ –C ₁₁	1.384	1.381	1.395	1.419	1.390	1.409
N ₂ –C ₉	1.350	1.330	1.371	1.390	1.345	1.342
N ₂ –C ₁₀	1.350	1.330	1.371	1.390	1.346	1.351
Ru–N ₂	2.108	2.296	2.083	2.161	2.278	2.219
Ru–N ₃	2.177	2.269	2.176	2.222	2.270	2.241
Ru–N ₄	2.177	2.269	2.177	2.222	2.270	2.241
Ru–N ₅	2.176	2.268	2.176	2.222	2.269	2.241
Ru–N ₆	2.176	2.268	2.177	2.222	2.269	2.241
Ru–N ₇	2.195	2.265	2.194	2.233	2.266	2.263
dihedral angle	38.7	47.7	32.7	43.1	42.2	33.7

(b)

C ₁ –N ₁	1.473	1.481	1.487	1.521	1.496	1.481
C ₂ –N ₁	1.353	1.334	1.368	1.382	1.349	1.358
C ₆ –N ₁	1.347	1.332	1.364	1.386	1.354	1.357
C ₂ –C ₃	1.370	1.370	1.383	1.411	1.373	1.372
C ₅ –C ₆	1.374	1.363	1.386	1.408	1.378	1.371
C ₃ –C ₄	1.408	1.396	1.421	1.434	1.406	1.416
C ₄ –C ₅	1.405	1.403	1.418	1.438	1.412	1.418
C ₄ –C ₇	1.447	1.467	1.454	1.482	1.467	1.451
C ₇ –C ₈	1.354	1.333	1.368	1.385	1.345	1.355
C ₈ –C ₉	1.432	1.459	1.441	1.469	1.462	1.454
C ₉ –C ₁₀	1.358	1.333	1.372	1.389	1.345	1.353
C ₁₀ –C ₁₁	1.431	1.459	1.441	1.468	1.462	1.465
C ₁₁ –C ₁₂	1.355	1.333	1.369	1.386	1.345	1.348
C ₁₂ –C ₁₃	1.446	1.468	1.453	1.481	1.469	1.486
C ₁₃ –C ₁₄	1.406	1.399	1.419	1.438	1.408	1.401
C ₁₃ –C ₁₇	1.407	1.396	1.420	1.436	1.406	1.405
C ₁₄ –C ₁₅	1.379	1.373	1.390	1.415	1.383	1.394
C ₁₆ –C ₁₇	1.378	1.375	1.390	1.414	1.384	1.394
N ₂ –C ₁₅	1.351	1.336	1.371	1.392	1.351	1.347
N ₂ –C ₁₆	1.354	1.332	1.374	1.390	1.348	1.352
Ru–N ₂	2.106	2.246	2.091	2.144	2.236	2.375
Ru–N ₃	2.172	2.267	2.173	2.220	2.269	2.248
Ru–N ₄	2.172	2.267	2.173	2.220	2.269	2.273
Ru–N ₅	2.171	2.267	2.174	2.220	2.268	2.273
Ru–N ₆	2.171	2.267	2.174	2.220	2.268	2.273
Ru–N ₇	2.203	2.278	2.200	2.241	2.276	2.276

^a Atoms in the compounds are enumerated as it is shown in the structures above the corresponding section. All geometries are calculated in the gas phase excluding those presented in the last column.

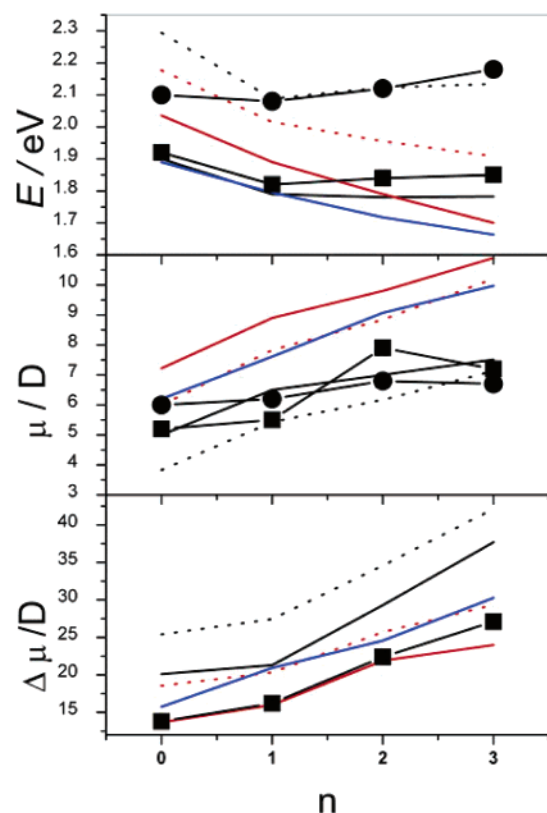


Figure 2. Values of $\Delta\mu$, μ , and E : experimental^{11–14} (■ – Stark spectroscopy, ● – UV–visible absorption) and calculated for HF (black lines), B3P86 (red lines), and MP2 (blue line) optimized structures. Solid and dotted lines correspond to molecular geometries obtained by LanL2DZ and 6-311++g(d,p)/LanL2DZ basis sets, respectively.

compounds in solution gives a steadily increasing of this value that is in good agreement with experiment.¹²

The variation in results obtained using different methods of structure optimization is caused by the distinction between the BLA values and the Ru(NH₃)₅-ligand distances. The former effect is well-known,^{26,27} and to clarify the influence of the latter one on the excited-state properties structure **2** was optimized by the HF approach using the CEP-4G basis set on the Ru and the LanL2DZ one on all other atoms. Obtained molecular geometry demonstrates that all bond lengths are identical with the HF/LanL2DZ optimized structure but that the Ru(NH₃)₅-ligand distance is 0.015 Å longer. At the same time the difference between Ru(NH₃)₅-ligand distances for the HF/LanL2DZ/6-311++g(d,p) and HF/CEP-4G/LanL2DZ optimized structures coincide with an accuracy of 0.002 Å and have a different BLA. Comparing the results of TD-B3P86/6-311++g(d,p)/LanL2DZ analysis for these structures (Table 3) it is seen that the effect of the Ru(NH₃)₅-ligand distance variation is smaller than the BLA variation but not negligible. In the considered case elongation of the Ru(NH₃)₅-ligand bond has the same effect as the BLA increasing. As a result, the discrepancy between the experimental and the theoretical data obtained by employing the different method optimized geometries is caused by a variation of both BLA and Ru(NH₃)₅-ligand distances.

From Table 1 it is seen that the BLA values for all compounds are quite the same, but the Ru(NH₃)₅-ligand

Table 3. Experimental^{11–14} and Theoretical Values of E , μ , and $\Delta\mu$ Obtained by TD-B3P86 Analysis Using Different Basis Sets^a

salt	E	μ	$\Delta\mu$	optimization method
1	2.1	6.0		MeCN (exp.)
	1.92	5.2	13.8	PrCN (exp.)
	1.90	5.0	20.1	HF/LanL2DZ
	1.94	4.27	23.41	HF/LanL2DZ ^b
	2.17	4.43	23.10	HF ^c
	2.29	3.83	25.40	HF/6-311++g(d,p)/LanL2DZ
	2.04	7.22	13.67	B3P86/LanL2DZ
	2.18	5.99	18.55	B3P86 /6-311++g(d,p)/LanL2DZ
	1.89	6.20	15.75	MP2/LanL2DZ
	2.08	6.2		MeCN (exp.)
2	1.82	5.5	16.2	PrCN (exp.)
	1.79	6.5	21.3	HF/LanL2DZ
	1.88	5.43	26.77	HF/LanL2DZ ^b
	2.03	5.89	25.44	HF ^c
	2.04	5.72	26.09	HF ^d
	2.09	5.43	27.43	HF/6-311++g(d,p)/LanL2DZ
	1.89	8.90	16.00	B3P86/LanL2DZ
	2.02	7.83	20.31	B3P86 /6-311++g(d,p)/LanL2DZ
	1.80	7.61	20.94	MP2/LanL2DZ
	2.12	6.8		MeCN (exp.)
3	1.84	7.9	22.4	PrCN (exp.)
	1.78	7.0	29.3	HF/LanL2DZ
	1.79	6.89	29.75	HF/LanL2DZ ^b
	2.04	6.62	32.82	HF ^c
	2.12	6.17	34.57	HF/6-311++g(d,p)/LanL2DZ
	1.79	9.80	21.91	B3P86/LanL2DZ
	1.96	8.84	25.69	B3P86 /6-311++g(d,p)/LanL2DZ
	1.72	9.07	24.57	MP2/LanL2DZ
	2.18	6.7		MeCN (exp.)
	1.85	7.2	27.1	PrCN (exp.)
4	1.78	7.51	37.68	HF/LanL2DZ
	1.85	5.98	34.44	HF/LanL2DZ ^b
	2.06	7.63	43.08	HF ^c
	2.13	7.13	42.15	HF/6-311++g(d,p)/LanL2DZ
	1.70	10.90	24.02	B3P86/LanL2DZ
	1.91	10.21	29.35	B3P86 /6-311++g(d,p)/LanL2DZ
	1.66	9.97	30.27	MP2/LanL2DZ

^a In all cases the used basis set is the same as that employed for the geometry optimization one, except as otherwise noted. ^b Optimized by the HF/LanL2DZ method in the MeCN solution. ^c Electronic transitions were calculated by the 6-311++g(d,p)/LanL2DZ basis set using the HF/LanL2DZ optimized structures. ^d Same as c for the HF/CEP-4G/LanL2DZ optimized structure.

distances are varied for structures **1**, **2**, and **4**. The comparative analysis of TD-B3P86 results obtained at the HF/LanL2DZ method using optimization in the gas phase and the MeCN solution (Table 3) indicates that the calculated values of E , μ , and $\Delta\mu$ are not systematically improved by including the solvent effect in the optimization procedure. Since for solute optimized structures Ru(NH₃)₅-ligand distances are not equilibrium, we can say only about the qualitative effect of this geometry parameter on investigated properties. Thus, the accurate estimation of the Ru(NH₃)₅-ligand distance could have an affect on the electronic excitation properties of considered chromophores.

Values of ground-state dipole moments μ_g are also strongly influenced by solvent. The absolute values of μ_g of consid-

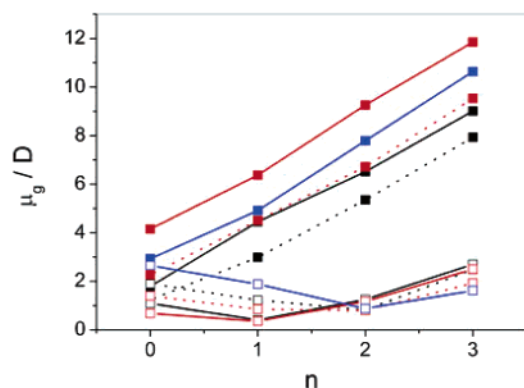


Figure 3. Calculated values of the ground-state dipole moment μ_g for investigated compounds in the gas phase (open symbols) and the MeCN solution (solid symbols). μ_g were estimated by the B3P86 method for the HF (black), B3P86 (red), and MP2 (blue) optimized structures. Solid and dotted lines denote data obtained by LanL2DZ and 6-311++g(d,p)/LanL2DZ basis sets, respectively.

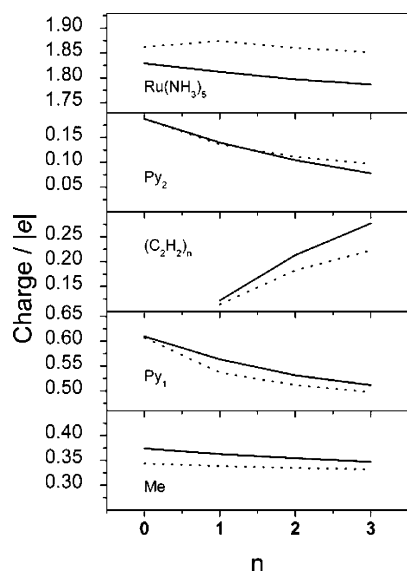


Figure 4. B3P86/LanL2DZ NPA calculated charges in the gas phase (solid lines) and the MeCN solution (dotted lines) for the chemical groups constituting compounds **1–4**.

ered complexes in solution are larger than in the gas phase and also depend on both the way of molecular geometry optimization and used basis set. B3P86 calculations of μ_g for structures optimized by different methods are summarized in Figure 3. NPA results for ground-state charge distribution in the gas phase and the MeCN solution are presented in Figure 4 and illustrate MLCT in considered chromophores. We have also compared results for $\Delta\mu$ calculated by FF and one particle RhoCI density approach. The results of the B3P86 calculations of $\Delta\mu$ by one particle RhoCI density method are presented in Figure 5. For the B3P86 optimized structures in the gas phase the results obtained in the present work and published in a paper (see ref 13) are quite the same. The calculated $\Delta\mu(n)$ in MeCN solution demonstrates the same tendency of change like the experimental one but is approximately two times overestimated, and the FF calculation method is more accurate.

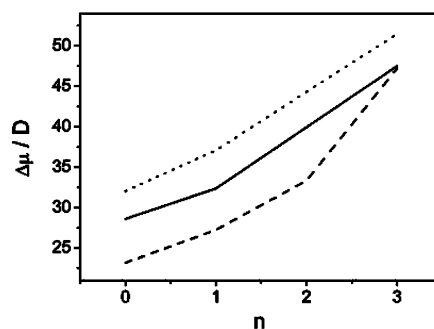


Figure 5. Difference between ground and excited states dipole moments $\Delta\mu$ calculated in MeCN solute by one particle RhoCI density for structures optimized by HF/LanL2DZ (solid), HF/6-311++g(d,p)/LanL2DZ (dotted), and B3P86/LanL2DZ methods (dashed). TD-B3P86 analysis in each case was performed using the same basis set that was used for structure optimization.

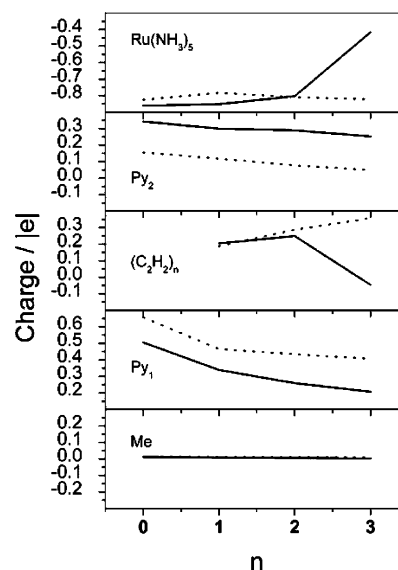


Figure 6. B3P86/LanL2DZ NPA calculated ground-to-excited-state ICT in the gas phase (solid lines) and the MeCN solution (dotted lines) for the chemical groups constituting compounds Me-Py₁-(C₂H₂)_n-Py₂-Ru(NH₃)₅ **1–4**. Py₁ and Py₂ denote the pyridinium rings attached to Me and Ru(NH₃)₅ groups, respectively.

The calculations of ground-to-excited-state charge transfer was performed by subtraction of NPA calculated excited-state charge distribution from the same value for the ground state. Obtained results are plotted in Figure 6. It is seen that solvent intensifies the ground-to-excited-state charge transfer on the Py₁ group and reduces it on the Py₂ one for all investigated complexes. For compound **4** this charge transfer is about two times larger in solution for the Ru(NH₃)₅ group and significantly larger and has an opposite sign for the polyene chain. To illustrate this, the structures of molecular orbitals for investigated complexes both in the gas phase and the MeCN solution are plotted in Figure 7. For compounds **3** and **4** the MLCT transition is caused by the (HOMO-3, HOMO) → LUMO transition in the gas phase and the HOMO → LUMO one in solution, while for structures **1** and **2** the HOMO → LUMO transition takes place in both media. For structures **1** and **2** HOMO and LUMO are

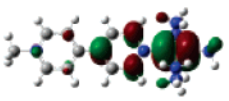
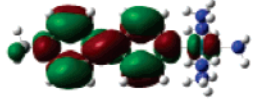
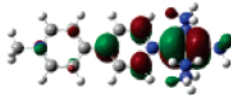
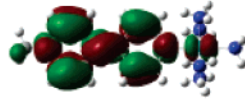
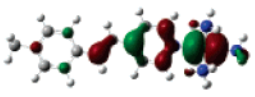
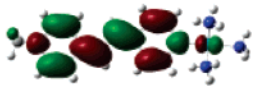
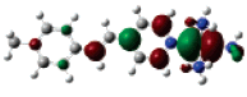
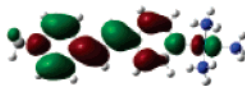
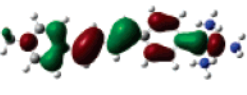

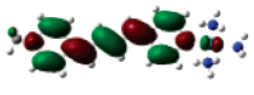


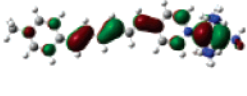


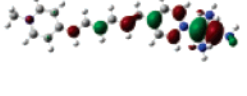

Salt	Gas phase		MeCN solution	
	Ground state	Excited state	Ground state	Excited state
[1]				
[2]				
[3]	 			
[4]	 			

Figure 7. Electron density contours calculated for the MOs involved in the ICT transitions of the cations **1–4** in both the gas phase and the MeCN solute.

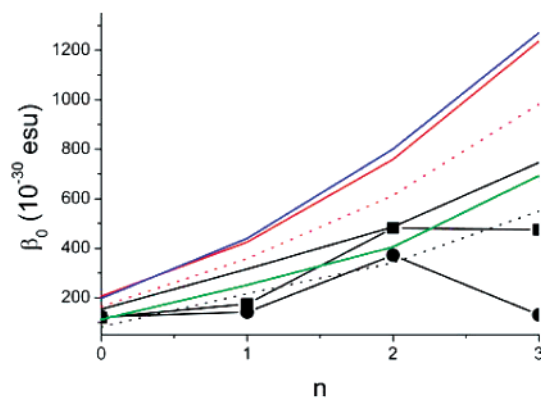
quantitatively the same and HOMO presents a larger electron density around the metal group, and the LUMO mostly lies on the acceptor part of the molecule in both the gas phase and the MeCN solution (see Figure 4). The same picture is for solute compounds **3** and **4**, but in the gas phase the HOMO-3 and HOMO spread over the whole molecule. This fact explains the large discrepancy between the gas phase and the solution calculated values of $\Delta\mu$. The interaction with the solvent leads to polarization of molecules and molecular dipole moment increases. As it is shown in Figure 6, ground-to-excited ICT also intensifies for structures **3** and **4** that leads to an increasing of excited-state dipole moment too. These two solvent effects on electronic structures of ground and excited states give significant growth of the $\Delta\mu$ in solution compared to the gas phase.

Values of β_0 calculated by eq 1 for considered cases of different optimization methods and basis sets are plotted in Figure 8. The HF/6-311++g(d,p)/LanL2DZ calculated $\beta_0(n)$

is in the best agreement with experiment. The HF/LanL2DZ optimized structures with the following TD-B3P86/6-311++g-(d,p)/LanL2DZ analysis also give very good results for all compounds excluding structure **4**, but even in this case agreement with the experiment it is better than for all other methods. These results demonstrate that excitation properties of compounds investigated are significantly dependent on the molecular geometry. As it was shown above, the structures optimized by the HF, B3P86, and MP2 methods give different relationships between bond lengths. The electron–electron correlations taken into consideration by the MP2 approach give the molecular structures that give the values of E , μ , $\Delta\mu$, and β_0 that are not in good agreement with the experiment. The HF and B3P86 optimized structures are sufficiently close to each other, but details of molecular geometry lead to some differences in electronic excitation properties. The HF optimized structures demonstrate good agreement with the experiment for $E(n)$ and $\Delta\mu(n)$, while

Table 4. Calculated Values of E , μ , $\Delta\mu$, and β_0 for the New Palladium-Based Organometallic Chromophore (Structure 6) in Comparison with the Ru(II) Ammine Complex with the Same Length of the Polyene Chain (Structure 2) for the Gas Phase (MeCN Solution)

salt	$E(\text{eV})$	$\mu(\text{D})$	$\Delta\mu(\text{D})$	$\beta_0(10^{-30} \text{ esu})$	basis set
2	2.65 (1.82)	4.89 (6.34)	20.59 (22.19)	82 (315)	LanL2DZ
6	2.75 (2.92)	10.36 (10.63)	8.85 (14.07)	147 (218)	LanL2DZ
2	2.94 (2.09)	4.60 (5.43)	21.12 (27.43)	60 (216)	LanL2DZ/6-311++g(d,p)
6	2.72 (2.88)	10.98 (11.56)	7.14 (10.34)	136 (195)	LanL2DZ/6-311++g(d,p)

**Figure 8.** Experimental (■ – Stark spectroscopy, ● – hyper-Rayleigh scattering^{12,13}) and estimated by eq 1 values of β_0 . Calculated data are presented for HF (black lines), B3P86 (red lines), and MP2 (blue line) optimized structures. Solid and dotted lines denote results obtained by LanL2DZ and 6-311++g(d,p)/LanL2DZ basis sets, correspondingly. Results for HF/LanL2DZ optimized structures that were analyzed by the TD-B3P86/LanL2DZ/6-311++g(d,p) approach are plotted by the green line.

the B3P86 ones give the best agreement for $\mu(n)$. Since in TSM the β_0 is the linear function of $\Delta\mu$ and the quadratic one of μ , the calculation of the value of β_0 by the HF optimized structures is more preferable.

In a short description, the proposed method of a new organometallic NLO active compound design is the HF/6-311++g(d,p)/LanL2DZ geometry optimization with the following TD-B3P86/6-311++g(d,p)/LanL2DZ analysis of electronic excitation properties. The value of $\Delta\mu$ has to be calculated by the FF approach. To keep the computation time the molecular structure optimization may be performed by the HF/LanL2DZ method. As it was shown above, the results obtained by this manner are close to properties predicted for the HF/6-311++g(d,p)/LanL2DZ optimized structures. The proposed approach has a restriction to be taken into account during consideration of the push–pull chromophores with long π -conjugated chains. As it was demonstrated,²⁸ the density functional theory fails for linear and nonlinear responses in the case of polyene chains with $n > 6$, and some other theoretical approaches have to be used in this situation. In our case use of the B3P86 method is applicable since the maximal length of the investigated chain (n) was smaller than 6. In the next section we use the developed approach to predict a new perspective organometallic chromophore.

Design of a New NLO Active Compound. As an example of using the proposed application for design of an organometallic compound with a high value of β_0 , we present a study of a new palladium-based NLO active compound (see

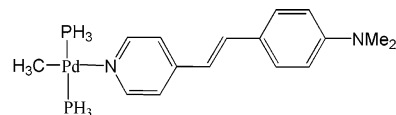
**Figure 9.** New palladium-based NLO active organometallic chromophore with a predicted large value of the first static hyperpolarizability (structure 6).

Figure 9). This is the stilbazolium cation where the one methyl group was replaced by the $\text{Pd}(\text{PMe}_3)_2\text{CH}_3$ ligand (structure 6). We optimized the design structure by the HF/LanL2DZ approach with the following TD-B3P86 analysis using both of the LanL2DZ and LanL2DZ/6-311++g(d,p) basis sets. The values of E , μ , $\Delta\mu$, and β_0 for the same level optimized structures for both the gas phase and the MeCN solution in comparison with the Ru(II) ammine complex with the same length of the polyene chain (structure 2) were calculated within the developed method, and the results are presented in Table 4. In opposite to the Ru(II) ammine complexes studied above a newly designed chromophore demonstrates blue-shifted solvatochromic effect. In the case of the soluted complex, the calculated β_0 value of the Pd complex is smaller than that of the Ru one for structure 2. However, in the gas phase the Pd complex has the larger value of β_0 as compared with the same value of the Ru complex. This is caused by a larger value of transition dipole moment μ . For practical application, it is important to know the characteristics of nonsoluted materials. Therefore, the results obtained for the Pd complex can suggest that metal substitution from Ru to Pd will improve the NLO properties of the organometallic compound.

Conclusion

We have presented the B3P86 study of the first singlet excited state of ruthenium(II) ammine complexes with a different number of polyene units. The solvent effect on the electronic structure in the framework of the PCM model has been studied. The TD-B3P86 study for HF, B3P86, and MP2 optimized structures has been carried out using the LanL2DZ and 6-311++g(d,p)/LanL2DZ basis sets, and calculated data were compared with experimental results. It is shown that in solution all considered compounds demonstrate not only significant red-shift of absorption energy maxima but also a sizable polarization of ground state and intensification of MLCT for low-lying excited states. Theoretical results are very sensitive to molecular geometry and basis set. The BLA and $\text{Ru}(\text{NH}_3)_5$ -ligand distances are important geometry parameters responsible for the electronic excitation properties. Using the HF/6-311++g(d,p)/LanL2DZ optimized structures with the following TD-B3P86/6-311++g(d,p)/

LanL2DZ treatment is found to be more preferable for the calculation of E , μ , and $\Delta\mu$ values in order to estimate the first static hyperpolarizability in the framework of TSM and is given the best agreement with the experiment. In comparison with the gas phase all investigated compounds demonstrate sizable polarization in the solution, and as a result the values of ground-state dipole moments in the solution are larger than the same values in the gas phase. For electronic excitation the solvent also intensifies the MLCT that leads to the increasing of $\Delta\mu$ in solution and the decreasing of this value in the gas phase. Using the FF method for calculation of $\Delta\mu$ gives better agreement with the experiment than one particle RhoCI density approach. Thus, the developed approach can be used to design a new perspective organometallic NLO active compound.

Acknowledgment. We thank the Information Science Group of the Institute for Materials Research, Tohoku University for their continuous support of the SR8000 supercomputing system. One of the authors (T. M. Inerbaev) was supported by JSPS Research Fellowship Grant No. P 04683.

References

- (1) *Nonlinear Optical Properties of Organic Molecules and Crystals*; Chemla, D. S., Zyss, J., Eds.; Academic Press: Orlando, FL, 1987.
- (2) *Introduction to Nonlinear Optical Effects in Molecules and Polymers*; Prasad, P. N., Williams, D. J., Eds.; Wiley: New York, 1991.
- (3) Verbiest, T.; Houbrechts, S.; Kauranen, M.; Clays, C.; Persoons, A. Second-Order Nonlinear Optical Materials: Recent Advances in Chromophore Design. *J. Mater. Chem.* **1997**, 7, 2175–2189.
- (4) Calabrese, J. C.; Cheng, L.-T.; Green, J. C.; Marder, S. R.; Tam, W. Molecular Second-Order Optical Nonlinearities of Metallocenes. *J. Am. Chem. Soc.* **1991**, 113, 7227–7232.
- (5) Le Bozec, H.; Renouard, T. Dipolar and Non-Dipolar Pyridine and Bipyridine Metal Complexes for Nonlinear Optics. *Eur. J. Inorg. Chem.* **2000**, 229–239.
- (6) Lacroix, P. G. Second-Order Optical Nonlinearities in Coordination Chemistry: the Case of Bis(salicylaldiminato)-metal Schiff Base Complexes. *Eur. J. Inorg. Chem.* **2000**, 229–239.
- (7) Qin, J.; Liu, D.; Dai, C.; Chen, C.; Wu, B.; Yang, C.; Zhan, C. Influence of the Molecular Configuration on Second-Order Nonlinear Optical Properties of Coordination Compounds. *Coord. Chem. Rev.* **1999**, 188, 23–34.
- (8) Long, N. J. Organometallic Compounds for Nonlinear Optics – The Search for Enlightenment! *Angew. Chem., Int. Ed. Engl.* **1995**, 34, 21–38.
- (9) Oudar, J. L.; Chemla, D. S. Hyperpolarizabilities of the Nitroanilines and Their Relations to the Excited-State Dipole Moment. *J. Chem. Phys.* **1977**, 66, 2664–2668.
- (10) Numerical prefactor in eq 1 can take values 6 or 3/2 instead 3. See: Willets, A.; Rice, J. E.; Burland, D. M. Problems in the Comparison of Theoretical and Experimental Hyperpolarizabilities. *J. Chem. Phys.* **1992**, 97, 7590–7599.
- (11) Coe, B. J.; Harris, J. A.; Brunschwig, B. S. Absorption Spectroscopic Studies of Dipolar Ruthenium (II) Complexes Possessing Large Quadratic Optical Responses. *J. Phys. Chem. A* **2002**, 106, 897–905.
- (12) Coe, B. J.; Jones, L. A.; Harris, J. A.; Brunschwig, B. S.; Asselberghs, I.; Clays, K.; Persoons, A. Highly Unusual Effects of π -Conjugation Extension of the Molecular Linear Quadratic Nonlinear Optical Properties of Ruthenium (II) Ammine Complexes. *J. Am. Chem. Soc.* **2003**, 125, 862–863.
- (13) Coe, B. J.; Jones, L. A.; Harris, J. A.; Brunschwig, B. S.; Asselberghs, I.; Clays, K.; Persoons, A.; Garin, J.; Orduna, J. Syntheses and Spectroscopic and Quadratic Nonlinear Optical Properties of Extended Dipolar Complexes with Ruthenium(II) Ammine Electron Donor and *N*-methylpyridinium Acceptor Groups. *J. Am. Chem. Soc.* **2004**, 126, 3880–3891.
- (14) Shin, Y. K.; Brunschwig, B. S.; Creutz, C.; Sutin, N. Electroabsorption Spectroscopy of Charge-Transfer States of Transition-Metal Complexes. 2. Metal-to-Ligand and Ligand-to-Metal Charge-Transfer Excited States of Pentaammineruthenium Complexes. *J. Phys. Chem.* **1996**, 100, 8157–8169.
- (15) Coe, B. J.; Chamberlain, M. C.; Essex-Lopresti, J. P.; Gaines, S.; Jeffery, J. C.; Houbrechts, S.; Persoons, A. Large Molecular Quadratic Hyperpolarizabilities in Donor/Acceptor-Substituted Trans-tetraammineruthenium(II) Complexes. *Inorg. Chem.* **1997**, 36, 3284–3292.
- (16) Kanis, D. R.; Lacroix, P. G.; Ratner, M. A.; Marks, T. J. Electronic Structure and Quadratic Hyperpolarizabilities in Organotransition-Metal Chromophores Having Weakly Coupled π -Networks. Unusual Mechanism of Second-Order Response. *J. Am. Chem. Soc.* **1994**, 116, 10089–10102.
- (17) Perdew, J. P. Density-Functional Approximation for the Correlation Energy of the Inhomogeneous Electron Gas. *Phys. Rev. B* **1986**, 33, 8822–8824.D.
- (18) Becke, A. D. Density-functional thermochemistry. III. The role of exact exchange. *J. Chem. Phys.* **1993**, 98, 5648–5652.
- (19) Frisch, M. J.; Trucks, G. W.; Schlegel, H. B.; Scuseria, G. E.; Robb, M. A.; Cheeseman, J. R.; Montgomery, J. A., Jr.; Vreven, T.; Kudin, K. N.; Burant, J. C.; Millam, J. M.; Iyengar, S. S.; Tomasi, J.; Barone, V.; Mennucci, B.; Cossi, M.; Scalmani, G.; Rega, N.; Petersson, G. A.; Nakatsuji, H.; Hada, M.; Ehara, M.; Toyota, K.; Fukuda, R.; Hasegawa, J.; Ishida, M.; Nakajima, T.; Honda, Y.; Kitao, O.; Nakai, H.; Klene, M.; Li, X.; Knox, J. E.; Hratchian, H. P.; Cross, J. B.; Adamo, C.; Jaramillo, J.; Gomperts, R.; Stratmann, R. E.; Yazyev, O.; Austin, A. J.; Cammi, R.; Pomelli, C.; Ochterski, J. W.; Ayala, P. Y.; Morokuma, K.; Voth, G. A.; Salvador, P.; Dannenberg, J. J.; Zakrzewski, V. G.; Dapprich, S.; Daniels, A. D.; Strain, M. C.; Farkas, O.; Malick, D. K.; Rabuck, A. D.; Raghavachari, K.; Foresman, J. B.; Ortiz, J. V.; Cui, Q.; Baboul, A. G.; Clifford, S.; Cioslowski, J.; Stefanov, B. B.; Liu, G.; Liashenko, A.; Piskorz, P.; Komaromi, I.; Martin, R. L.; Fox, D. J.; Keith, T.; Al-Laham, M. A.; Peng, C. Y.; Nanayakkara, A.; Challacombe, M.; Gill, P. M. W.; Johnson, B.; Chen, W.; Wong, M. W.; Gonzalez, C.; Pople, J. A. *Gaussian 03, Revision B.04*; Gaussian, Inc.: Pittsburgh, PA, 2003.
- (20) Mennucci, B.; Tomasi, J. Continuum solvation models: A new approach to the problem of solute's charge distribution and cavity boundaries. *J. Chem. Phys.* **1997**, 106, 5151–5158.

- (21) Wiberg, K. B.; Stratmann, R. E.; Frisch, M. J. A Time-Dependent Density Functional Theory Study of the Electronically Excited States of Formaldehyde, Acetaldehyde and Acetone. *Chem. Phys. Lett.* **1998**, 297, 60–64.
- (22) Cave, R. J.; Burke, K.; Castner, E. W., Jr. Theoretical Investigation of the Ground and Excited States of Courmarins 151 and Courmarin 120. *J. Phys. Chem. A* **2002**, 106, 9294–9305.
- (23) Reed, A. E.; Weinhold, F. Natural Bond Orbital Analysis of Near-Hartree–Fock Water Dimer. *J. Chem. Phys.* **1983**, 78, 4066–4073.
- (24) Reed, A. E.; Weinstock, R. B.; Weinhold, F. Natural Population Analysis. *J. Chem. Phys.* **1985**, 83, 735–746.
- (25) Reed, A. E.; Curtiss, L. A.; Weinhold, F. Intermolecular Interactions from a Natural Bond Orbital, Donor–Acceptor Viewpoint. *Chem. Rev.* **1988**, 88, 899–926.
- (26) Bourhill, G.; Brédas, J.-L.; Cheng, L.-T.; Marder, S. R.; Meyers, F.; Perry, J. W.; Tiemann, B. G. Experimental Demonstration of the First Hyperpolarizability of Donor–Acceptor-Substituted Polyenes on the Ground-State Polarization and Bond Length Alternation. *J. Am. Chem. Soc.* **1994**, 116, 2619–2620.
- (27) Meyers, F.; Marder, S. R.; Pierce, B. M.; Brédas, J.-L. Electric-Field Modulated Nonlinear-Optical Properties of Donor–Acceptor Polyenes – Sum-Over-States Investigation of the Relationship between Molecular Polarizabilities (α , β , and γ) and Bond Length Alternation. *J. Am. Chem. Soc.* **1994**, 116, 10703–10714.
- (28) Champagne, B.; Perpète, E. A.; van Gisbergen, S. J. A.; Baerends, E.-J.; Snijders, J. G.; Soubra-Ghaoui, C.; Robins, K. A.; Kirtman, B. Assessment of Conventional Density Functional Schemes for Computing the Polarizabilities and Hyperpolarizabilities of Conjugated Oligomers: An *Ab Initio* Investigation of Polyacetylene Chains. *J. Chem. Phys.* **1998**, 109, 10489–10498.

CT050193M